Superconducting state of very thin Pd films deposited on a diluted insulating $Eu_xSr_{1-x}S$ ferromagnet

Alexandr Cosceev,[1,*] Christoph Sürgers,[1,†] Hans-Gerd Boyen,[2] Peter Schweiss,[3] and Hilbert v. Löhneysen[1,3]

[1]*Karlsruhe Institute of Technology, Physikalisches Institut and DFG Center for Functional Nanostructures, P.O. Box 6980, D-76049 Karlsruhe, Germany*

[2]*Hasselt University, Institute for Materials Research, B-3590 Diepenbeek, Belgium*

[3]*Karlsruhe Institute of Technology, Institut für Festkörperphysik, P.O. Box 3640, D-76021 Karlsruhe, Germany*

(Received 7 April 2011; published 26 May 2011)

The electronic transport in very thin Pd films deposited on insulating $Eu_xSr_{1-x}S$ ($0 \leqslant x \leqslant 1$) is investigated. The temperature dependent resistance $R(T)$ of films with $d_{Pd} \geqslant 14$ nm shows metallic behavior and a logarithmic increase toward low temperatures characteristic of (anti-)localization and electron-electron interaction effects also observed for Pd films on Si(111). Films with $d_{Pd} = 7$ nm are superconducting below a transition temperature T_c which decreases with increasing Eu concentration from $T_c = 0.9$ K for $x = 0$ to $T_c < 50$ mK for $x = 1$. The origin of superconductivity in the thin Pd films is presumably due to the formation of an interfacial Pd-S alloy and/or to a charge transfer at the Pd/$Eu_xSr_{1-x}S$ interface. The decrease of T_c vs x is attributed to the magnetic pair breaking of the ferromagnetic $Eu_xSr_{1-x}S$ underneath. The $R(T)$ behavior of films with $d_{Pd} \geqslant 10$ nm suggests that these are not superconducting or have a strongly reduced T_c presumably due to the proximity effect of the nonsuperconducting S-free upper part of the Pd film.

DOI: 10.1103/PhysRevB.83.174516 PACS number(s): 74.25.fc, 73.20.Fz, 73.40.Ns, 74.62.Bf

I. INTRODUCTION

Interfaces between solids have a profound scientific and technological importance, as exemplified by field-effect transistors which form the basis of today's information technology. Recently, a new class of interfaces between materials where the electrons interact strongly with each other have become of considerable interest. In particular, interfaces involving transition-metal oxides have received close scrutiny. Among the more important findings is the observation of an interfacial metallic layer between $LaAlO_3$ and $SrTiO_3$ that even becomes superconducting under stringent conditions of sample thickness.[1–3]

Transition-metal layers themselves offer a wealth of interesting phenomena. Among the elemental transition metals, palladium takes a unique position. It is very close to a ferromagnetic instability because of the large electronic density of states $N(E_F)$ at the Fermi level E_F and, thus, a large Stoner enhancement factor. Minute additions of Fe render Pd ferromagnetic, with a critical concentration $x_c \approx 0.01$ at %.[4] Moreover, Pd may become ferromagnetic in thin films or in nanoparticles due to the expansion of the crystalline lattice. In free-standing Pd films, ferromagnetism is predicted due to the formation of quantum-well states and the concurrent modification of the electronic density of states.[5] On the other hand, many Pd compounds and alloys are superconducting, including H-implanted Pd films.[6] Particularly noteworthy is the observation of bulk superconductivity in $Pd_{70}Zr_{30}$ metallic glasses.[7] Hence, Pd is very susceptible to superconductivity induced by minor modifications of the electron density or electronic structure. In all these instances, superconductivity is believed to be conventional, that is, mediated by electron-phonon coupling leading to an *s*-wave order parameter. In contrast, *p*-wave superconductivity was predicted for Pd[8] but until now has not been observed, possibly due to pair breaking by nonmagnetic impurities.[9]

Here we report on the electronic transport properties of thin Pd films in search for superconductivity. In order to investigate whether possible superconductivity is conventional or unconventional, we chose an insulating substrate with varying degrees of magnetic order. In this work we have chosen $Eu_xSr_{1-x}S$, a magnetic semiconductor becoming insulating at low temperatures and allowing tuning of the magnetic properties by variation of the Eu concentration x. We find that the Pd films exhibit a resistance increase with decreasing temperature T due to weak antilocalization and electron-electron interaction effects as reported earlier for thin Pd and superconducting PdH_x films.[10,11] More importantly, we find that very thin Pd films on $Eu_xSr_{1-x}S$ are superconducting below 1 K. The superconductive transition temperature T_c decreases monotonically with increasing Eu concentration x consistent with pair breaking of Cooper pairs with *s*-wave symmetry.

II. EXPERIMENT

Epitaxial $Eu_xSr_{1-x}S$ films were deposited on Si(111) in ultra-high vacuum (UHV) (base pressure below 3×10^{-8} mbar). The Si(111) substrate (*p* type, $\rho = 15\ \Omega$ cm, 1×2 cm^2) was chemically cleaned and the native oxide was stripped off by a buffered HF solution leaving an H-terminated Si-H surface. The Si-H layer was removed by heating the substrate in UHV to a substrate temperature $T_S = 1070$ K. Powders of EuS and SrS were mixed together to obtain the desired concentration x and were evaporated from an electron-beam-heated tungsten crucible. 50 nm $Eu_xSr_{1-x}S$ was deposited on the Si(111) surface at $T_S = 1100$ K at a rate of 0.3–0.4 Å/s. Previous work has shown that stoichiometry of EuS is approached with increasing $T_S > 800$ K.[12] The morphology of a $Eu_{0.55}Sr_{0.45}S$ film was checked by atomic force microscopy in the contact mode (not shown) yielding an average corrugation of ≈1 nm with single protrusions of ≈2 nm height.

Subsequently, the substrate was cooled to ≈330 K and a Pd strip (width $w = 1$ mm, length $L = 12$ mm) of thickness $d_{Pd} = 7$–30 nm was deposited onto the $Eu_xSr_{1-x}S$ film through

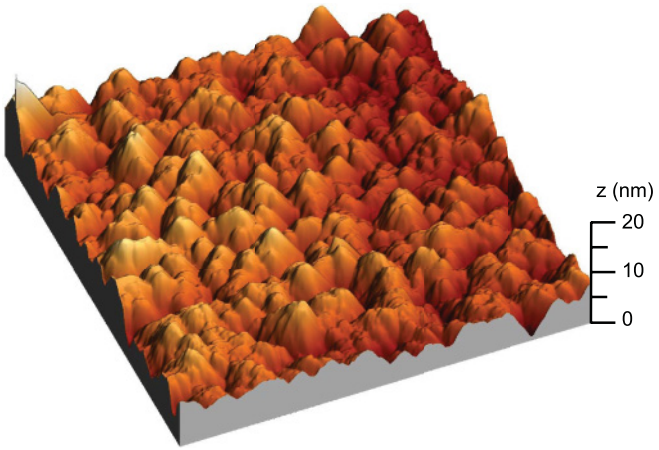

FIG. 1. (Color online) STM image of 7-nm Pd on 50-nm SrS obtained in constant-current mode. Image size 250 nm × 250 nm, bias voltage 2 V, tunneling current 80 pA.

a mechanical mask by electron-beam evaporation at a rate of 0.4–0.5 Å/s. All film thicknesses are nominal as determined with a quartz-crystal monitor and do not take corrugation and surface roughness into account. The STM image of 7 nm Pd on SrS (Fig. 1) obtained in the constant-current mode shows a granular growth of connected islands with an average diameter of 3 nm. This is in agreement with the three-dimensional Vollmer-Weber growth reported for transition metals deposited on oxide substrates (MgO, ZnO) and semiconductors (MoS_2, GaAs).[13] Finally, four 15-nm thick Pd contacts were deposited on the strip for resistance measurements. To investigate the electric-field effect, the Pd strip was covered by a 30-nm SiO_2 film for electrical insulation followed by three separated 15-nm thick Pd contacts serving as source, drain, and gate. In addition, a Pd film ($d_{Pd} = 7$ nm) was deposited directly on Si(111) without a $Eu_xSr_{1-x}S$ interlayer as a reference sample. Thin copper wires were glued to the contacts by conductive silver paste for four-point resistance measurements performed in a ^{4}He and in a ^{3}He bath cryostat each equipped with a superconducting solenoid providing magnetic fields B up to 5 and 18 T, respectively. In addition, the resistance of a sample with $x = 1$ was measured in a dilution refrigerator down to 50 mK. From R the sheet resistance $R_\square = Rw/L = \rho/d_{Pd}$ (ρ: resistivity) was obtained.

Structural characterization was done by x-ray diffraction (θ–2θ scan) with a two-circle diffractometer in Bragg-Brentano focusing using Cu K_α radiation ($\bar{\lambda}_{K\alpha} = 1.5418$ Å) employing a graphite monochromator in the diffracted beam to reduce the contribution from the K_β line, and with a four-circle diffractometer using Cu $K_{\alpha 1}$ radiation ($\lambda_{K\alpha 1} = 1.54056$ Å).

Magnetic hysteresis loops $M(B)$ were recorded with a SQUID magnetometer at $T = 2.5$ K. The magnetic ac susceptibility χ was determined with the sample placed in one of two pick-up coils, both surrounded by a primary coil providing the ac magnetic field. The second (empty) pick-up coil was used for compensation of the background signal.

The chemical properties of the samples were characterized by Auger electron spectroscopy (AES) and x-ray photoelectron spectroscopy (XPS) *ex situ*. Auger electron spectra were recorded with a cylindrical mirror analyzer and an electron excitation energy of 2 keV. Photoemission spectra of the Pd-3d and S-2p lines were excited by Al K_α radiation ($E =$ 1486.6 eV) and detected with a hemispherical analyzer.

III. RESULTS

A. Structural and chemical characterization

Figure 2 shows a θ–2θ scan demonstrating the epitaxial growth of cubic $Eu_{0.55}Sr_{0.45}S$ (space group $Fm3m$) in (111) orientation. The (200), (220), and (311) Bragg reflections are not observed due to the (111) fiber texture along the growth direction. The inset shows the lattice parameter $a = \sqrt{3}\,d_{111}$ calculated from the lattice-plane distance $d_{111} = \lambda/2\sin\theta$ for three films of different x. The $a(x)$ dependence is in good agreement with previous data obtained on bulk $Eu_xSr_{1-x}S$ crystals[14] and with data of pure EuS ($a = 5.967$ Å) and pure SrS ($a = 6.024$ Å).[15]

Figure 3 shows the diffractogram of Pd films with different d_{Pd} deposited on SrS obtained in the four-circle diffractometer. The strong (111) reflection of the Si substrate was reduced by tilting the sample 4° off from the Bragg reflection. For $d_{Pd} = 30$ and 15 nm the diagrams indicate a growth of polycrystalline Pd with lattice parameters in good agreement with values expected for bulk Pd. For thinner films, the Pd peaks could not be resolved from the background.

The chemical composition of the bilayer was measured by Auger depth profiling on a 7-nm Pd film on SrS, exploiting clear Auger signals from Pd, Sr, and S in the low-energy range 0–550 eV [see Fig. 4(a)] without a contribution from oxygen ($E_O = 512$ eV). Figure 4(b) shows the depth profile, that is,

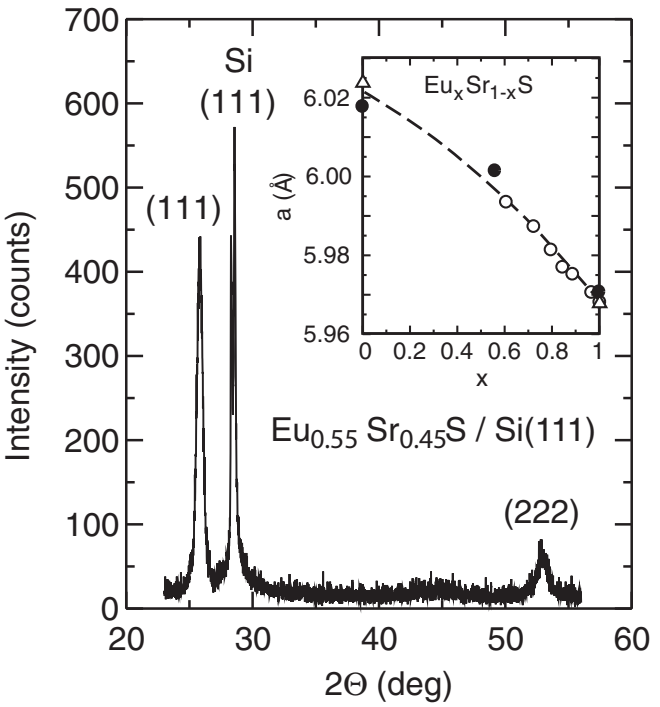

FIG. 2. X-ray θ–2θ scan ($\bar{\lambda}_{K\alpha} = 1.5418$ Å) of 50 nm $Eu_{0.55}Sr_{0.45}S$ on Si(111). Inset shows the lattice constant a determined from the (111) lattice plane distance d_{111} by $a = \sqrt{3}\,d_{111}$ vs concentration x (solid symbols). Open circles and triangles indicate data from Refs. 14 and 15, respectively, dashed line serves as guide to the eye.

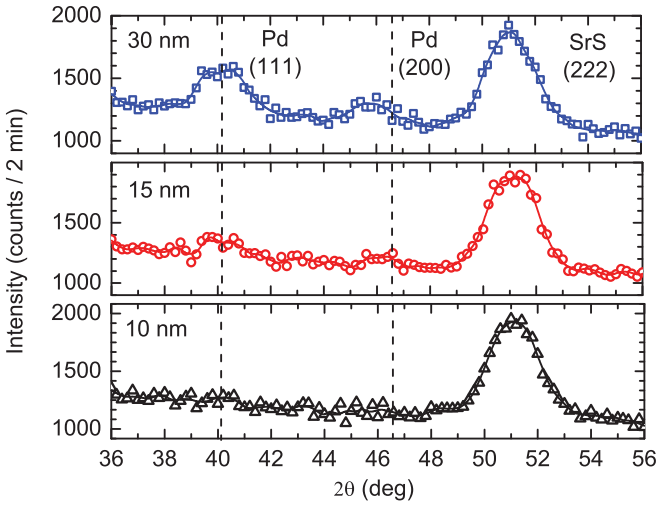

FIG. 3. (Color online) X-ray scan ($\lambda_{K\alpha 1} = 1.54056$ Å) of Pd films of different thickness d_{Pd} on SrS(111). The Si substrate was rotated 4° off from the Si(111) Bragg reflection to reduce the background intensity arising from the strong Si(111) peak. Dashed lines indicate the positions of (111) and (200) Bragg peaks for bulk Pd.

Auger signals vs sputtering time t, obtained while Ar^+ was sputtering. The transition width $\Delta t \approx 2$ min (corresponding to $\Delta z = 4$ nm Pd) at the Pd-S interface is of the order of the depth resolution of our system. The width Δt is defined as the difference of the time coordinate t between 84% and 16% of the intensity change at the interface.[16] In addition, an interdiffusion of Pd and S might occur across the interface. Furthermore, a sulfur signal is found on top of the Pd film ($t \approx 0$–1 min) [see also Fig. 4(a)] indicating a segregation of S from SrS across the thin Pd layer. This appears possible since the segregation of S dissolved in Pd was observed earlier.[17] Alternatively, the S signal could arise from Auger electrons escaping from SrS regions which are not covered by Pd due to the grain growth of Pd (see Fig. 1).

In order to check the possible presence of S in the Pd film, XPS spectra were recorded close to the S 2p level (see Fig. 5). Pd films of different thickness on SrS show a broad peak around $E = 163$ eV arising from PdS. For the thinnest film ($d_{\mathrm{Pd}} = 5$ nm) the spectrum can be described by a superposition of contributions arising from sulfur compounds

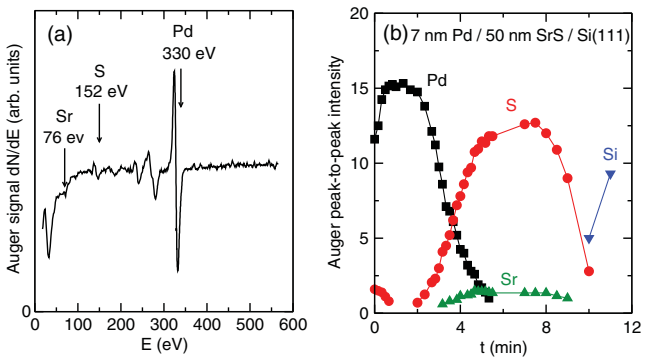

FIG. 4. (Color online) (a) Auger electron spectrum of 7-nm Pd on SrS. (b) Auger depth profile obtained by sputtering the sample with 1 keV Ar^+ ions while recording the Auger spectra (a).

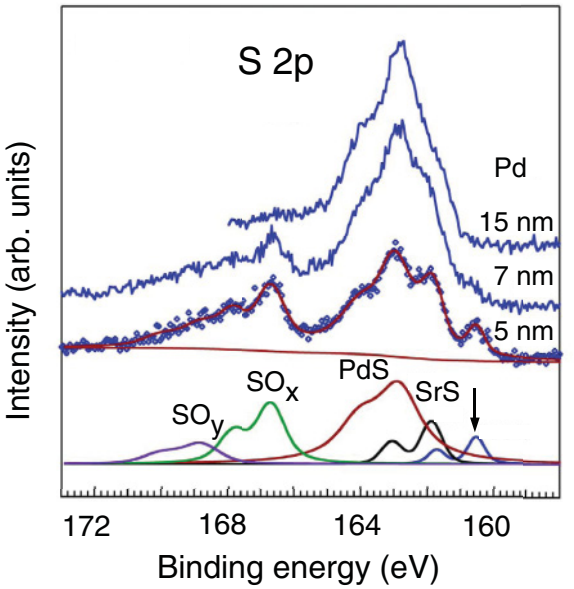

FIG. 5. (Color online) XPS spectra of Pd films of different thickness d_{Pd} on SrS. Solid lines show a fit to the data for the 5-nm film and the fitted background. The bottom part shows the individual contributions of various oxides and sulfides to the total spectrum derived from the XPS database.[18] Arrow indicates a Pd-S contribution of unknown composition which is not found in the database.

SO_x, PdS, and SrS taken from the NIST data base.[18] In addition, an intensity maximum at 160.5 eV is observed for the 5-nm Pd film which is not found in the database and is therefore attributed to the formation of an unknown Pd-S compound. This signal is quickly suppressed with increasing d_{Pd}. For $d_{\mathrm{Pd}} = 7$ nm, it turns into a shoulder and cannot be resolved anymore for $d_{\mathrm{Pd}} = 15$ nm. The peak arising from SO_x increases with decreasing film thickness. These XPS data support the assumption that a reaction between Pd and S occurs at the interface.

B. Magnetic properties of $Eu_xSr_{1-x}S$ films

EuS is a II–VI semiconductor with a direct band gap $E_g = 1.7$ eV at room temperature and exhibits isotropic 3D Heisenberg ferromagnetism with a Curie temperature $T_C = 16.5$ K. Substitution of Eu by nonmagnetic Sr results in a magnetic phase diagram shown in Fig. 6(a). The magnetic properties of $Eu_xSr_{1-x}S$ can be tuned by variation of the Eu concentration x from nonmagnetic SrS to ferromagnetic EuS (Curie temperature $T_C = 16.5$ K) via isolated magnetic clusters ($x < 0.125$),[19] spin glass ($0.125 \leqslant x \leqslant 0.51$),[20] and reentrant ferromagnetism ($x > 0.51$).[21] SrS is more akin to an insulator with an indirect band gap of 2.7 eV and a chemical potential close to the top of the valence band.[22]

The magnetic properties of 50-nm $Eu_xSr_{1-x}S$ films were characterized by SQUID magnetometry and ac-susceptibility measurements. Figure 6(b) shows the $M(H)$ hysteresis loop of EuS on Si(111) at $T = 2.5$ K characteristic of a ferromagnet with a coercivity of $B \approx 20$ mT. The Curie temperature T_C of ferromagnetic films with different x was determined from the extrapolation of the reciprocal ac-susceptibility $\chi^{-1}(T)$ to $\chi^{-1}(T_C) = 0$ [see Fig. 6(c)]. The spin-glass freezing

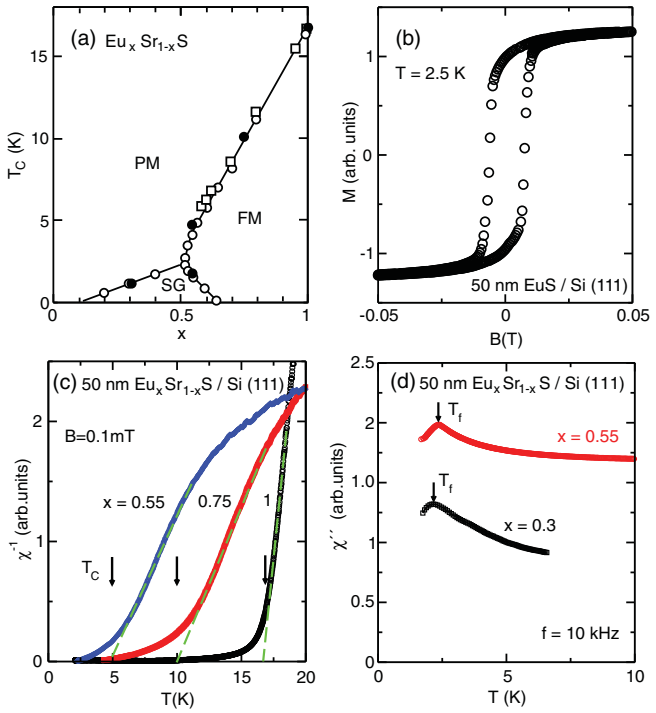

FIG. 6. (Color online) (a) Magnetic phase diagram of $Eu_xSr_{1-x}S$. PM: paramagnet; FM: ferromagnet; SG: spin glass. Open circles for $Eu_xSr_{1-x}S$ bulk samples from Ref. 21, open squares for EuS/SrS multilayers from Ref. 23, closed circles from this work. (b) Magnetic hysteresis $M(B)$ of 50-nm EuS on Si(111) at $T = 2.5$ K. (c) Reciprocal magnetic susceptibility $\chi^{-1}(T)$ of 50-nm $Eu_xSr_{1-x}S$ for different concentrations x. T_C indicates the Curie temperature determined from the extrapolation of the linear T dependence to $\chi^{-1} = 0$ (dashed lines). (d) Imaginary part $\chi''(T)$ of the ac susceptibility. T_f indicates the spin-glass freezing temperature determined from the maximum of $\chi''(T)$.

temperature T_f of samples with smaller x was determined from the maximum in the imaginary part χ" of χ [see Fig. 6(d)]. All values are in good agreement with the phase diagram obtained for bulk $Eu_xSr_{1-x}S$[21] and EuS/SrS multilayers[23] [see closed circles in Fig. 6(a)]. $Eu_xSr_{1-x}S$/Si(111) "substrates" with $x = 0$ and $x = 0.55$ were checked to be insulating at 4.2 K.

C. Resistance of thin Pd films on Si(111)

The resistance of a 7-nm Pd film deposited on Si(111) without a $Eu_xSr_{1-x}S$ interlayer was measured for comparison. Figure 7(a) shows the temperature dependence of the sheet resistance $R_\square(T)$. For temperatures $T > 150$ K the resistance is very small due to the shorting by the semiconducting Si substrate [see inset Fig. 7(a)]. Below $T = 100$ K, $R_\square(T)$ decreases linearly with decreasing temperature until it rises again. The semilogarithmic plot shows that below 4 K a $-\ln T$ behavior is observed. From the residual resistance $R_\square = 58.1\ \Omega$ (resistivity $\rho = 40.6\ \mu\Omega$ cm) an electronic mean free path $l = 5$ nm shorter than the film thickness was estimated using $\rho l = 2 \times 10^{-5}\ \mu\Omega\,\mathrm{cm}^2$.[10] The magnetoresistance (MR) $\Delta R_\square(B)/R_\square^2 = [R_\square(B) - R_\square(0)]/R_\square^2$ for magnetic fields B applied in the film plane is plotted vs $\ln B$ in Fig. 7(b). The

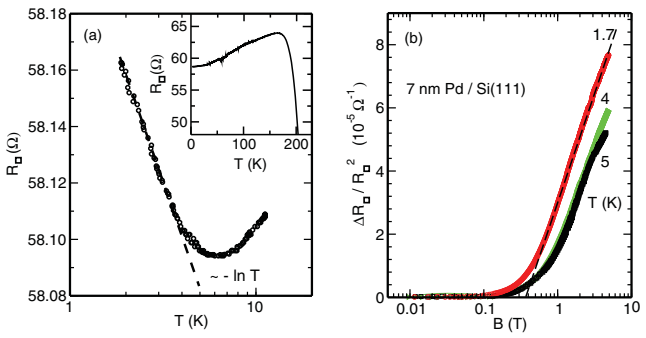

FIG. 7. (Color online) (a) Sheet resistance $R_\square$ vs $\ln T$ of 7-nm Pd on Si(111). Dashed line shows a behavior $R_\square \propto -\ln T$. Inset shows a linear $R(T)$ plot for higher temperatures. (b) Semilogarithmic plot of the magnetoresistance of 7-nm Pd on Si(111) in parallel magnetic field for different temperatures T. Dashed line shows a behavior $R_\square \propto \ln B$.

MR is positive up to the maximum field and increases with decreasing temperature.

Similar behavior of $R_\square(T)$ and $\Delta R_\square(B)/R_\square^2$ for thin and/or and quench-condensed Pd films was reported earlier by several groups and attributed to weak antilocalization (due to the strong spin-orbit scattering in Pd) and enhanced electron-electron interaction in a two-dimensional disordered metal.[10,11,24–27] In principle, these different contributions could be disentangled by comparing the MR behavior in perpendicular and parallel magnetic fields.

We did not observe indications for a superconducting transition due to the formation of a Pd-Si interface alloy. Such a transition was reported earlier for 3–5 nm Pd films on Si(111)[10,24] and was signalized by a negative MR below ~10 K. Furthermore, it is important to mention that we did not observe indications of superconductivity for Pd films $d_{Pd} = 2$, 4, 5, 7, and 20 nm prepared under similar conditions on MgO(001) and KBr substrates. In all those samples we observed below 10 K an increasing resistance with decreasing temperature down to 1.7 K and a positive MR. Because of the large *positive* MR, a contribution from the Kondo effect, which also would give rise to a $-\ln T$ behavior, can be ruled out.

D. Pd films on $Eu_xSr_{1-x}S$

1. Resistance

Figure 8 shows the temperature dependence of the resistance normalized to the minimum resistance $R_0(T = 8\ \mathrm{K})$ for Pd films of different thickness d_{Pd} on SrS/Si(111). For $d_{Pd} = 30$ and 14 nm, the rise of R toward lower temperatures is similar to the behavior observed for the 7-nm Pd film on Si(111). However, for a lower thickness of 7 nm the resistance suddenly drops for $T < 2.5$ K suggesting the onset of superconductivity. This was investigated in detail in the following.

Figure 9 shows $R_\square(T)$ in perpendicular magnetic fields up to 5 T for 7-nm Pd films deposited on (a) SrS and (b) $Eu_{0.55}Sr_{0.45}S$. The sudden drop of $R_\square(T)$ below 2.5 K in zero field is observed for the Pd film on $Eu_{0.55}Sr_{0.45}S$ as well. With increasing field, the temperature below which the resistance

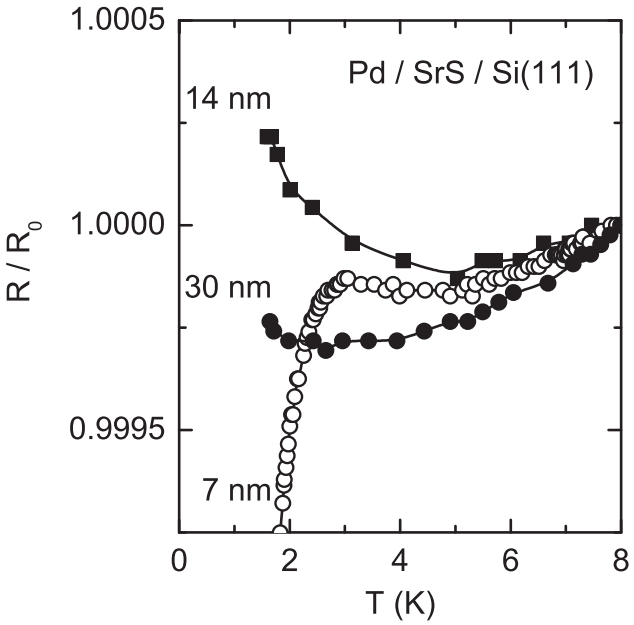

FIG. 8. Scaled resistance $R/R_0(T = 8\,\mathrm{K})$ vs T for Pd films of different thickness d_{Pd} on SrS. $R_0 = 692.85\ \Omega$ (7 nm), 231.11 Ω (14 nm), and 42.52 Ω (30 nm).

drops shifts toward lower temperatures and a maximum evolves at a temperature T^*. Eventually the logarithmic increase observed for thicker Pd films (Fig. 8) is reestablished. The field dependence of T^* [inset Fig. 9(a)] suggests that the sudden drop is due to a superconductive transition. This is indeed confirmed by measurements performed in a ^{3}He cryostat down to $T = 0.3$ K. Figures 10 and 11 show the resistively measured superconductive transitions for 7-nm Pd films on SrS and on $Eu_{0.55}Sr_{0.45}S$, respectively, in (a) parallel and (b) perpendicular magnetic fields. In zero field, transition temperatures $T_c = 0.9$ K ($x = 0$) and $T_c = 0.67$ K ($x = 0.55$) were measured. T_c is defined as the temperature where R has dropped to 50% of its normal state resistance. Hence the behavior shown in Fig. 9 is reminiscent of a transition from superconductivity to localization in a disordered metal.

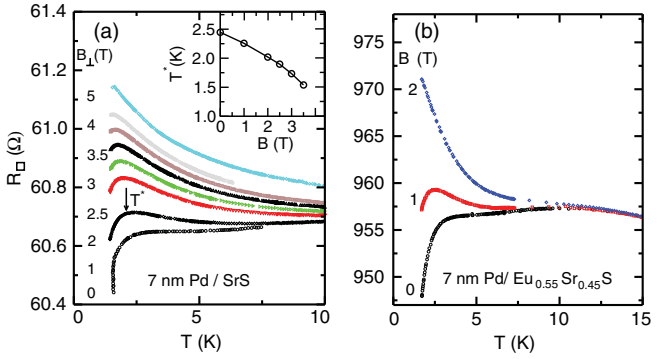

FIG. 9. (Color online) (a) Sheet resistance $R_{\square}(T)$ for 7-nm Pd on SrS in perpendicular magnetic fields. Inset shows the field dependence of the temperature T^* where the maximum occurs in $R_{\square}(T)$. (b) $R_{\square}(T)$ for 7-nm Pd on $Eu_{0.55}Sr_{0.45}S$ in perpendicular magnetic fields.

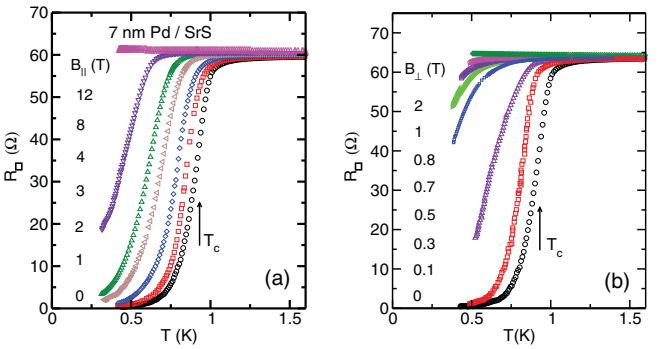

FIG. 10. (Color online) Resistive superconductive transitions $R_{\square}(T)$ in (a) parallel and (b) perpendicular magnetic fields for 7-nm Pd on SrS. The superconductive transition temperature T_c is indicated by arrows.

From the resistive superconducting transitions in magnetic field, the superconducting phase diagram is obtained. Figure 12 shows the upper critical fields B_{c2} for both orientations. Fits to the experimental data were obtained with the functions[28]

$$B_{c2\perp} = \frac{\Phi_0}{2\pi\xi_{\mathrm{GL}}^2(0)}\left(1 - \frac{T}{T_c}\right), \tag{1}$$

$$B_{c2\parallel} = \frac{\sqrt{12}\Phi_0}{2\pi\xi_{\mathrm{GL}}(0)d}\sqrt{1 - \frac{T}{T_c}}, \tag{2}$$

where $\Phi_0 = h/2e$ is the superconductive flux quantum and $\xi_{\mathrm{GL}}(0)$ is the Ginzburg-Landau coherence length at zero temperature. Equation (2) is valid for $d < \xi(0)$. The superconductive parameters T_c and $\xi_{\mathrm{GL}}(0)$ determined from the fits to the data close to T_c (dashed lines) are summarized in Table I where indeed $d = 7\ \mathrm{nm} \leqslant \xi_{\mathrm{GL}}$ is found, except for $T_S = 77$ K. Using $\xi_{\mathrm{GL}}(0)$ determined from $B_{c2\perp}$ [Eq. (1)], the fit with Eq. (2) yields an estimate of the thickness d of the superconducting part which agrees within ±30% with the nominal thickness. Since the resistivity $\rho = 42\ \mu\Omega$ cm of the 7-nm film Pd on SrS is similar to $\rho = 40\ \mu\Omega$ cm for the 7-nm Pd film on Si(111) (Sec. III C) we assume a similar mean free path $l = 5$ nm. This allows an estimation of the BCS coherence length ξ_0. In the dirty limit $\xi_{\mathrm{GL}}(0) = 0.855\,(l\,\xi_0)^{1/2}$,[28] yielding $\xi_0 = 93$ nm for the superconducting Pd film on SrS.

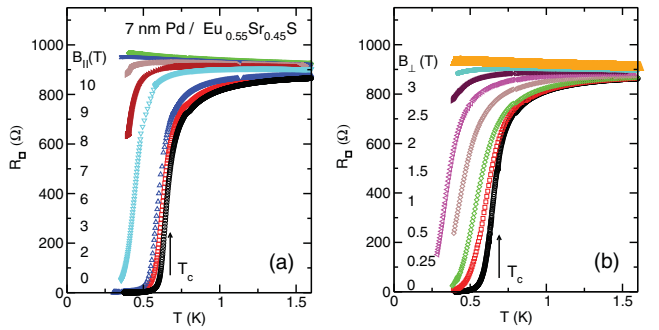

FIG. 11. (Color online) Resistive superconductive transitions $R_{\square}(T)$ in (a) parallel and (b) perpendicular magnetic fields for 7-nm Pd on $Eu_{0.55}Sr_{0.45}S$. The superconductive transition temperature T_c is indicated by arrows.

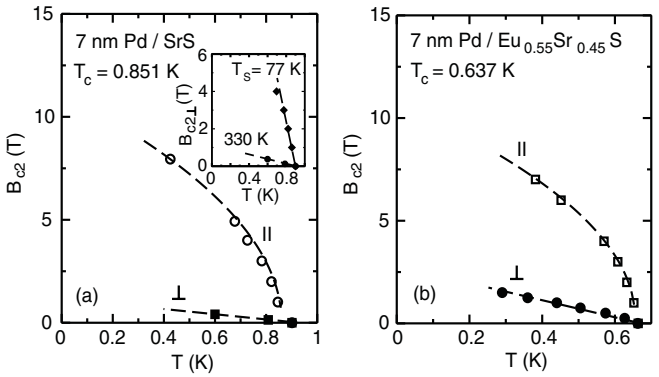

FIG. 12. Parallel and perpendicular upper critical magnetic fields $B_{c2}(T)$ of 7 nm Pd on (a) SrS and (b) $Eu_{0.55}Sr_{0.45}S$. Dashed lines indicate a linear and square-root behavior for the perpendicular and parallel field orientation, respectively. Inset (a) shows the behavior of $B_{c2\perp}(T)$ for films prepared at substrate temperatures $T_S = 330$ K and $T_S = 77$ K.

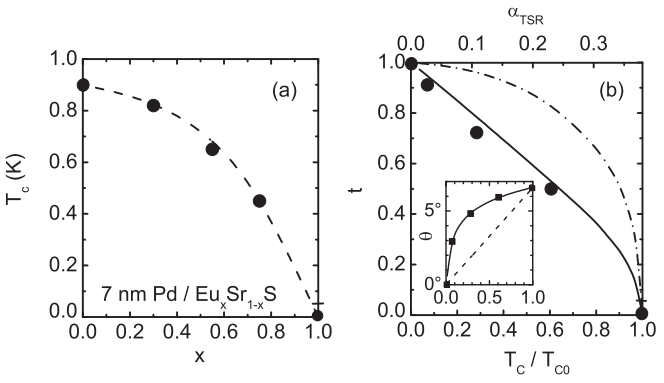

FIG. 13. (a) $T_c(x)$ of 7-nm Pd on $Eu_xSr_{1-x}S$. Dashed line serves as guide to the eye. For $x = 1$, no superconducting transition was found down to 50 mK. (b) Scaled transition temperature $t = T_c/T_{c0}$ vs scaled Curie temperature. Solid line shows the universal functional behavior obtained from the Abrikosov-Gor'kov theory[38] for a pair-breaking parameter α_{AG} taken as the reduced Curie temperature $T_C(x)/T_C(x = 1)$. Dash-dotted curve represents $t(\alpha_{TSR})$ indicating pair breaking by the proximity of superconducting Pd to an insulating ferromagnet.[39] Inset shows the spin-mixing angle θ vs T_C/T_{C0}, see text for details. Dashed line shows a linear behavior that would arise from $t(\alpha_{TSR})$ plotted in the main frame (dash-dotted curve).

Superconductivity in $R_\square(T)$ was observed for 7-nm Pd films on $Eu_xSr_{1-x}S$ with other Eu concentrations except for $x = 1$. Figure 13(a) shows that $T_c(x)$ decreases monotonically with increasing x, and for $x = 1$ no superconducting transition was observed down to the lowest achievable temperature $\approx$50 mK of a ^{3}He/^{4}He dilution refrigerator.

For Pd films on $Eu_xSr_{1-x}S$ with $x > 0$, the resistance is much larger than for those with $x = 0$ (cf. Fig. 9). We speculate that this might be due to increased surface roughness. In order to check directly whether the induced superconductivity is due to disorder effects, a 7-nm Pd film was deposited on SrS at a reduced $T_S = 77$ K. The deposition at low temperature and the reduced adatom mobility results in an enhanced structural disorder, as deduced from an increased $R_\square = 318\ \Omega$ compared to 60.7 Ω obtained for $T_S = 330$ K, and in a larger slope of $B_{c2}(T)$ due to the smaller $\xi_{GL}(0) = 4.5$ nm and electronic mean free path [see inset Fig. 12(a)]. However, both films showed the same $T_c = 0.85$ K (Table I) indicating that the effect of disorder on induced superconductivity in our samples requires further investigation.[29] We mention that a 7-nm Pd film deposited on SrS at high $T_S = 870$ K did not show a superconducting transition possibly due to a strongly enhanced interface reaction between Pd and SrS or due to a different growth behavior. This was not investigated further.

2. *Hall effect and electric-field effect*

A positive Hall voltage was measured on the 7-nm Pd film on $Eu_{0.55}Sr_{0.45}S$ at $T = 2$ K in a magnetic field up to 18 T with a linear magnetic-field dependence yielding a Hall constant $R_H = 2.9 \times 10^{-11}$ m^3/A s and a hole concentration of $n_h = 2.1 \times 10^{22}$ cm^{-3}. This is somewhat smaller than $R_H = 12 \times 10^{-11}$ m^3/A s reported for bulk Pd.[30] In Pd, the Hall coefficient changes its sign from negative for bulk Pd to positive in thin films at $d_{Pd} \approx 13$ nm due to the different thickness dependences of the electron and hole mobilities in a two-band model as briefly reported by Panchenko *et al.*[31]

TABLE I. Superconductive parameters of 7-nm Pd films on $Eu_xSr_{1-x}S$ obtained from the fits of the upper critical fields (cf. Fig. 12). n.d.: $B_{c2\parallel}$ not determined.

x	T_S (K)	$R_\square$ (Ω)	ρ ($\mu\Omega$ cm)	T_c (K)	$\xi_{GL}(0)$ (nm)	d (nm)
0	77	318	223	0.85	4.5	n.d.
0	330	60.7	42	0.851	19.9	4.9
0.55	330	957	670	0.637	10.3	10.7

The electric-field effect was measured on a 7-nm Pd film on $Eu_{0.55}Sr_{0.45}S$ with an additional Pd top gate as described in Sec. II. For this sample, $T_c = 0.6$ K was found in agreement with T_c of the sample mentioned above, which demonstrates the reproducible sample preparation and the formation of a superconducting phase. Figure 14 shows the source-drain resistance $R_{SD}(T)$ for different gate voltages U_G. For negative $U_G = -10$ V, the steep decrease of the resistance at T_c remains almost unchanged with respect to $U_G = 0$. However, even for small positive $U_G = 0.05$ V a "foot" appears just below T_c. For higher positive U_G up to 40 V, T_c remains constant but the "residual" resistance below T_c increases monotonically. The residual resistance R_{SD} below T_c is shown in the inset of Fig. 14 indicating a steep increase of R_{SD} just above zero gate voltage and an apparent saturation at high U_G for $T = 0.3$ K. In the normal state, R_{SD} is independent of U_G. This allows a switching of the device between the fully and partly superconducting state by the positive gate voltage.

Generally, the field-induced change of the charge carrier concentration Δn is given by[32]

$$\Delta n = \frac{\epsilon_{SiO_2}\,\epsilon_0\,U_G}{e\,d_{Pd}\,d_{SiO_2}} \tag{3}$$

(ϵ_0 is the electric field constant, $\epsilon_{SiO_2} = 3.9$). The increase of the residual resistance with increasing positive gate voltage may indicate the presence of positive charge carriers (holes) that are depleted from the interface region in agreement with the positive Hall coefficient. We obtain a small change of the

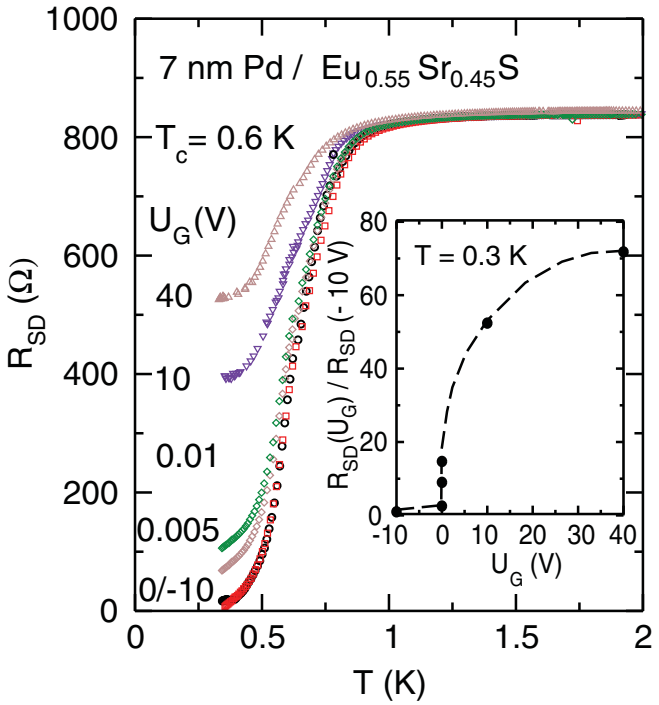

FIG. 14. (Color online) Source-drain resistance $R_{SD}(T)$ of 7-nm Pd on $Eu_{0.55}Sr_{0.45}S$ for various gate voltages U_G. Inset shows the scaled $R_{SD}(U_G)/R_{SD}(U_G = -10\ \text{V})$ in the superconducting state. Dashed line is a guide to the eye.

hole concentration $n_h \approx 10^{18}\ \text{cm}^{-3}$ for $U_G = 40$ V. However, a detailed understanding of the generation of the "residual" resistance below T_c and its dependence on U_G is lacking.

IV. DISCUSSION

A. Resistivity in the normal state

The electronic transport of thin disordered or quench-condensed Pd films on various substrates has been studied earlier by several groups.[10,11,24–27,33–35] The most detailed analysis was done by Markiewicz *et al.*[10,24] providing evidence that the electronic transport is strongly influenced by weak antilocalization (WAL) and enhanced electron-electron interaction (EEI) in a two-dimensional system. In the present case $k_F l \gg 1$, with $k_F = 4.55\ \text{nm}^{-1}$,[10] justifying the application of the pertubative theory.[36] d_{Pd} is shorter than the thermal coherence length $L_T = (\hbar/3v_F l k_B T)^{-1/2}$, $L_T(10\ \text{K}) = 20\ \text{nm}$, thus the film can be considered as two-dimensional concerning electron-electron interaction. Here we have used a Fermi velocity $v_F = 5.3 \times 10^5$ cm/s which was estimated by taking into account the large s–d interband scattering.[10] The temperature dependence of the corresponding correction to the sheet resistance for a two-dimensional system with respect to the Drude term is[36]

$$\frac{\Delta R_\square(T)}{R_\square^2} = -L_{00}\left[\alpha p + \left(1 - \frac{3}{4}\tilde{F}_\sigma\right)\right]\ln\frac{T}{T_0} = \beta \ln\frac{T}{T_0}, \tag{4}$$

where $L_{00} = e^2/2\pi^2\hbar = 1.233 \times 10^{-5}\ \Omega^{-1}$, α takes into account the strong ($\alpha = -1/2$) or weak ($\alpha = 1$) spin-orbit scattering, and $\tilde{F}_\sigma$ the electron screening parameter, $0 \leqslant \tilde{F}_\sigma \leqslant 1$ for strong or weak electron screening, respectively. p is the exponent of the temperature-dependent dominant inelastic scattering mechanism (electron-phonon, electron-electron, or spin-flip scattering) $\tau_{in} \propto T^{-p}$ responsible for the dephasing. The first term in Eq. (4) arises from WAL and the second term from EEI.

For our 7-nm Pd film on Si(111) the slope $\beta = -2.4 \times 10^{-5}\ \Omega^{-1}$ of the logarithmic behavior [cf. Fig. 7(a)] is in good agreement with earlier results $\beta = -2.6 \times 10^{-5}\ \Omega^{-1}$ for 3-nm Pd film on Si,[10] $\beta = -2 \times 10^{-5}\ \Omega^{-1}$ for 2.5–10 nm films on glass.[11] However, it is impossible to obtain meaningful parameters for α, p, and $\tilde{F}_\sigma$ if one tries to separate β into two contributions due to WAL and EEI.[36] p is usually considered to be $p = 3$ for electron-phonon scattering and $p = 2$ for electron-electron scattering. Assuming $\tilde{F}_\sigma \geqslant 0$ results in $\alpha > 0.32$ ($p = 3$) or $\alpha > 0.48$ ($p = 2$) in contrast to $\alpha = -1/2$ expected for the strong spin-orbit scattering in Pd as reported earlier in various experiments. Vice versa, assuming $\alpha = -1/2$ leads to a negative value of $\tilde{F}_\sigma \approx -3$ which is not accounted for by theory.

In principle, the different contributions arising from WAL and EEI can be disentangled by MR measurements in parallel and perpendicular magnetic fields for different temperatures.[36] Usually the MR in parallel fields is much smaller than in perpendicular fields. For strong spin-orbit scattering the MR in parallel field due to EEI is negligible small because both the orbital part and the spin-splitting part are absent. The latter arises from the strong spin-orbit scattering that mixes the spin channels.[10,36] The MR due to WAL is positive for small fields and turns negative for larger fields. In the present case, in parallel field the MR of the 7-nm Pd film on Si(111) is positive for all temperatures and shows a logarithmic behavior $\Delta R_\square(B)/R_\square^2 = \gamma \ln(B/B_0)$ with $\gamma = 3.2 \times 10^{-5}\ \Omega^{-1}$ [see Fig. 9(b)]. This is larger than $\gamma = 10^{-5}\ \Omega^{-1}$ (Refs. 27 and 10) reported earlier for the MR measured in *perpendicular* fields. This strong positive MR in parallel field which is even larger than obtained in previous investigations in perpendicular filed is incompatible with the theory for EEI and WAL. As already reported by Bergmann,[37] Pd stands out as a metal where even an infinite strength of spin-orbit scattering does not reproduce the experimental results. This is presumably due to the vicinity of Pd to ferromagnetic order originating from the large Stoner enhancement factor and leading to spin fluctuations.

In view of the similar behavior of both $\Delta R_\square(T)$ and the MR obtained for Pd on Si[10,24] and for thick Pd films on $Eu_xSr_{1-x}S$ reported here, we refrain from a detailed analysis and determination of the temperature dependence of the individual electron scattering lengths. In the following we focus on the 7-nm Pd films deposited on $Eu_xSr_{1-x}S$ which clearly show superconducting behavior with T_c decreasing for increasing Eu concentration x.

B. Superconductivity

We first discuss the dependence of the superconductive transition temperature on the Eu concentration of the $Eu_xSr_{1-x}S$ substrate. The reduction of T_c by pair-breaking processes such as magnetic fields or magnetic impurities is

usually characterized by a pair-breaking parameter α_{AG} in the Abrikosov-Gor'kov (AG) theory.[38] Figure 13(b) shows the reduced transition temperatures $t = T_c/T_{c0}$ vs T_C/T_{C0} of all samples together with the universal behavior obtained from the AG theory assuming that $\alpha_{AG} \propto T_C/T_{C0}$. T_{c0} is the transition temperature for the sample with $x = 0$ and T_{C0} is the Curie temperature for the sample with $x = 1$.

A more adequate description for the present case of a magnetic insulator was given by Tokuyasu, Sauls, and Rainer (TSR)[39] who considered a thin superconducting film of thickness $d < \xi_0$ sandwiched between a magnetic and a nonmagnetic insulator. The model was previously applied to GdN/NbN.[40] The spins of quasiparticles impinging on and reflected from the superconductor/magnet interface are rotated by a spin-mixing angle θ. This magnetic scattering at the magnetic interface destroys superconductivity even for $\theta \ll 1$ usually found for rare-earth compounds.[39] In general, θ depends on the projection of the spin on the surface normal for every trajectory. The reduced superconductive transition temperature decreases with increasing pair-breaking parameter α_{TSR}, where $\alpha_{TSR} = \xi_0 \tan(\theta/2)/2d$. For $\alpha_{TSR} = \alpha_{TSR,c} = 0.3816$ superconductivity is completely suppressed ($t = 0$). Figure 13(b) shows t vs α_{TSR} (dash-dotted line) taken from Ref. 39. For the values of ξ_0 and d of our superconducting films, $\tan(\theta/2)$ must be smaller than $2d\alpha_{TSR,c}/\xi_0 \approx 0.06$. Hence $\alpha_{TSR} \propto \theta$ would be expected. Clearly our data for the reduced superconductive transition temperature t are at variance with this expectation, if we assume that the spin-mixing angle scales linearly with the Curie temperature. An obvious explanation is that the assumption $\theta \propto T_C$ may be incorrect. Indeed, if we calculate θ within the TSR model from the measured t for Pd films on different $Eu_xSr_{1-x}S$ substrates, we obtain the $\theta(T_C/T_{C0})$ behavior shown in the inset of Fig. 13(b). This nonlinearity of $\theta(T_C/T_{C0})$ might reflect a different spin-mixing angle at a superconductor/spin glass compared to a superconductor/ferromagnet interface, with an apparently stronger pair breaking by the spin glass than by the ferromagnet. We note that a weakening of the pair breaking of thin Gd films on Nb was observed for continuous Gd films ($d_{Gd} \geqslant 2$ nm), vis-a-vis discontinuous, that is, magnetically disordered Gd films.[41]

Of course, strong pair breaking might also originate from diffusion of Eu into Pd. In this case, however, one might expect AG behavior that would scale with x instead of $\theta(T_C/T_{C0})$. Comparison of Figs. 13(a) and 13(b) shows, however, that AG scaling with $\theta(T_C/T_{C0})$ but *not* with x is observed.

The issue of different work functions and the variation of band alignment at the metal/nonmetal interface with concentration x was briefly explored. From photoemission data we obtained work functions $\phi = 4.7$ eV for a nonsuperconducting 7-nm Pd film on Si(111) and $\phi = 4.8$ eV for a superconducting 7-nm Pd film on SrS. Both values are somewhat lower than $\phi = 5.1$ eV reported for bulk Pd.[42] For p-type Si, SrS, and EuS different work functions of 4.6, 3.3, and 4.05 eV and Fermi level positions 0.24 eV, 0.9 eV, and $\approx$0 above the valence band, respectively, were estimated from Refs. 22,42–44. Hence, different electronic configurations are expected at the Pd/nonmetal interface. For Pd on p-type Si an accumulation layer in Si and a Schottky contact with a barrier of 1.0 eV is estimated. Pd in contact with SrS gives rise to an upward band bending and formation of a depletion layer in SrS with a Schottky barrier of 3.45 eV. An even stronger band bending and formation of a inversion layer in EuS with a barrier of 2.3 eV is expected for Pd on EuS. Here we have neglected the existence of interface states or metal-induced gap states which may be present. Our estimated values demonstrate that the electronic interface structure is possibly affected by the Eu concentration x in addition to the change of the magnetic properties. Comparison of the band bending estimated for Pd on SrS and on EuS suggests that T_c might decrease with increasing x due to a concentration-dependent band bending. However, whether this effect is more significant than the pair breaking would require a thorough investigation of the formation of interface or metal-induced gap states and of the barrier heights for different x.

We now discuss possible origins of superconductivity observed in very thin Pd films. As already mentioned above, superconductivity of Pd films on Si was found for thin Pd films of 3–5 nm thickness[24] due to the formation of Pd-Si interface alloy. In that case, a $T_c \approx 0.5$ K was measured on a 3-nm Pd film possibly fully transformed to Pd_2Si ($T_c \approx$ 0.25–0.5 K). For $d_{Pd} = 5$ nm, a residual resistivity was found well below T_c attributed to the formation of a bilayer of Pd on top of Pd_2Si, where the proximity effect of Pd drives some fraction of Pd_2Si normal.

In the present case the chemical characterization of our samples by XPS and AES suggests a chemical reaction that takes place at the interface between $Eu_xSr_{1-x}S$ and Pd, possibly forming a superconducting Pd-S compound of unknown composition. For thicker films superconductivity is suppressed by the proximity with the upper "S-free" part of the Pd film and reducing the pair amplitude in Pd-S. This can explain why in the present case no indications of superconductivity were found for 7-nm Pd on Si(111) (Sec. III C) much thicker than 3-nm Pd required for a complete transformation to Pd_2Si, and for Pd films on $Eu_xSr_{1-x}S$ with $d_{Pd} \geqslant 10$ nm (Sec. III D 1).

Superconductivity in binary $Pd_{2.2}S$ with $T_c = 1.63$ K was reported by Raub *et al.*[45] Furthermore, the binary palladium-sulfide phase diagram shows stable phases of tetragonal Pd_4S, cubic $Pd_{16}S_7$, and tetragonal PdS.[46] We prepared tetragonal PdS by heating a Pd film (on sapphire substrate) together with solid sulfur in a quartz tube under Ar atmosphere to 400 °C for several hours.[47,48] However, the fully reacted PdS film was not superconducting as inferred from resistance measurements down to $\approx$50 mK. Another possible candidate might be cubic $Pd_{16}S_7$ which can be considered as a metal with a resistivity $\rho \approx 720\ \mu\Omega\,$cm.[47] $Pd_{16}S_7$ is a precursor phase of PdS ($\rho > 10^4\ \mu\Omega\,$cm). A 370-nm thick Pd_4S film exhibits a resistivity $\rho = 16.5\ \mu\Omega\,$cm at room temperature with a linear temperature dependence characteristic of metallic conductivity.[49] Hence $Pd_{16}S_7$ and Pd_4S have to be investigated in the future in search for superconductivity in Pd-S compounds.

Superconductivity in our Pd films on SrS might also arise from electron charge transfer reducing $N(E_F)$. As shown in Fig. 14, we observe a decrease of the resistance jump at T_c upon applying a positive gate voltage to the Pd film, and a broadening yielding a finite residual resistance $R_0 \sim 0.63R_n$ at $V_G = 40$ V where R_n is the normal-state resistance just

above T_c. Negative gate voltages, on the other hand, did not alter the superconducting transition. Thus, a negative charge transfer from Pd to the $Eu_xSr_{1-x}S$ substrate may indeed be responsible for superconductivity. In line with this argument, we observe a positive Hall coefficient for our superconducting films. The issue remains what causes the charge transfer.

V. SUMMARY

The resistivity of Pd films deposited on $Eu_xSr_{1-x}S$ ($0 \leqslant x \leqslant 1$) shows strong deviations from the behavior of a clean metal due to the contribution of weak antilocalization and electron-electron interaction effects. Surprisingly, very thin films of 7-nm thickness become superconducting at a transition temperature T_c which decreases with increasing Eu concentration. The decrease of T_c vs x is attributed to the magnetic pair breaking of the ferromagnetic $Eu_xSr_{1-x}S$ substrate underneath. Concerning the origin of superconductivity two possibilities remain: (1) formation of an interfacial Pd-S layer of unknown stoichiometry and (2) strongly electronegative sulfur at the interface "binding" electrons. In both cases we expect superconductivity to be stable in only a small window of thickness, because for larger thickness the nonsuperconducting portion of the Pd film would suppress superconductivity in the thin layer adjacent to the $Eu_xSr_{1-x}S$ surface.

ACKNOWLEDGMENTS

We thank C. Pfleiderer for performing the measurements in the dilution refrigerator and A. Böttcher for sample characterization. This work was partly supported by the DFG Center for Functional Nanostructures (CFN) and the Federal Belgium Interuniversity Attraction Poles Program VI - 'Quantum effects in clusters and nanowires'.

*Present address: Institut für Materialien und Bauelemente der Elektronik, Leibniz Universität Hannover, Schneiderberg 39, D-30167 Hannover, Germany.

†christoph.suergers@kit.edu

[1] S. Thiel, G. Hammerl, A. Schmehl, C. W. Schneider, and J. Mannhart, Science **313**, 1942 (2006).

[2] N. Reyren, S. Thiel, A. D. Caviglia, L. Fitting Kourkoutis, G. Hammerl, C. Richter, C. W. Schneider, T. Kopp, A.-S. Rüetschi, D. Jaccard, M. Gabay, D. A. Muller, J.-M. Triscone, and J. Mannhart, Science **317**, 1196 (2007).

[3] A. D. Caviglia, S. Gariglio, N. Reyren, D. Jaccard, T. Schneider, M. Gabay, S. Thiel, G. Hammerl, J. Mannhart, and J.-M. Triscone, Nature (London) **456**, 624 (2008).

[4] C. Büscher, T. Auerswald, E. Scheer, A. Schröder, H. v. Löhneysen, and H. Claus, Phys. Rev. B **46**, 983 (1992).

[5] S. S. Ch. Hong, J. I. Lee, and R. Wu, Phys. Rev. B **75**, 172402 (2007), and references therein.

[6] B. Stritzker and W. Buckel, Z. Phys. B **257**, 1 (1972).

[7] J. E. Graebner, B. Golding, R. J. Schutz, F. S. L. Hsu, and H. S. Chen, Phys. Rev. Lett. **39**, 1480 (1977).

[8] D. Fay and J. Appel, Phys. Rev. B **16**, 2325 (1977).

[9] F. Pobell, Physica B+C **109-110**, 1485 (1982).

[10] R. S. Markiewicz and C. J. Rollins, Phys. Rev. B **29**, 735 (1984).

[11] L. Dumoulin, H. Raffy, P. Nedellec, D. S. MacLachlan, and J. P. Burger, Solid State Commun. **51**, 85 (1984).

[12] J. Köhne, G. Mair, N. Rasula, B. Saftic, and W. Zinn, J. Phys. (Paris) **41**, C5-127 (1980).

[13] A. Piednoir, E. Perrot, S. Granjeaud, A. Humbert, C. Chapon, and C. R. Henry, Surf. Sci. **391**, 19 (1997).

[14] K. Siratori, K. Kohn, H. Suwa, E. Kita, S. Tamura, F. Sakai, and A. Tasaki, J. Phys. Soc. Jpn. **51**, 2746 (1982).

[15] K. Syassen, Phys. Status Solidi A **91**, 11 (1985).

[16] S. Hofmann, in *Practical Surface Analysis*, edited by D. Briggs and M. P. Seah (Wiley, New York, 1990), Vol. 1.

[17] A. P. Dementjevand and O. P. Ivanova, Vacuum **45**, 901 (1994).

[18] NIST X-ray Photoelectron Spectroscopy Database [http://srdata.nist.gov/xps/].

[19] H. v. Löhneysen, Phys. Rev. B **22**, 273 (1980).

[20] H. Maletta and W. Felsch, Phys. Rev. B **20**, 1245 (1979).

[21] H. Maletta and W. Felsch, Z. Phys. B **37**, 55 (1980).

[22] A. Hasegawa and A. Yanase, J. Phys. C **13**, 1995 (1980).

[23] J. Wosnitza and H. v. Löhneysen, Europhys. Lett. **10**, 381 (1989).

[24] R. S. Markiewicz, C. J. Rollins, and J. S. Brooks, Surf. Sci. **142**, 56 (1984).

[25] S. Schmid-Marčić and J. Mydosh, Solid State Commun. **17**, 795 (1975).

[26] J. Kästner and H. v. Löhneysen, in *Anderson Localization*, edited by T. Ando and H. Fukuyama, Springer Proceedings in Physics, Vol. 28 (Springer, Berlin, 1988), p. 164.

[27] A. Carl, G. Dumpich, and D. Hallfarth, Phys. Rev. B **39**, 915 (1989).

[28] M. Tinkham, *Introduction to Superconductivity*, 2nd ed. (McGraw-Hill, New York, 1996).

[29] B. Stritzker, Phys. Rev. Lett. **42**, 1769 (1979).

[30] M. D. Wilding, Proc. Phys. Soc. **90**, 801 (1967).

[31] O. A. Panchenko, P. P. Lutsishin, and Yu. G. Ptushinskii, Zh. Eksp. Teor. Fiz. **56**, 134 (1969) [Sov. Phys. JETP **29**, 76 (1969)].

[32] J. Mannhart, Mod. Phys. Lett. B **6**, 555 (1992).

[33] G. Bergmann, Phys. Rev. Lett. **43**, 1357 (1979).

[34] W. C. McGinnis, M. J. Burns, R. W. Simon, G. Deutscher, and P. M. Chaikin, Physics B **107**, 5 (1981).

[35] G. Bergmann and G. Mathon, Solid State Commun. **55**, 521 (1985).

[36] P. A. Lee and T. V. Ramakrishnan, Rev. Mod. Phys. **57**, 287 (1985).

[37] G. Bergmann, Phys. Rep. **107**, 1 (1984).

[38] A. A. Abrikosov and L. P. Gor'kov, Zh. Eksp. Teor. Fiz. **39**, 1781 (1961) [Sov. Phys. JETP **12**, 1243 (1961)].

[39] T. Tokuyasu, J. A. Sauls, and D. Rainer, Phys. Rev. B **38**, 8823 (1988).

[40] J. Q. Xiao and C. L. Chien, Phys. Rev. Lett. **76**, 1727 (1996).

[41] C. Strunk, C. Sürgers, U. Paschen, and H. v. Löhneysen, Phys. Rev. B **49**, 4053 (1994).

[42] H. B. Michaelson, J. Appl. Phys. **48**, 4729 (1977).

[43] D. E. Eastman, F. Holtzberg, and S. Methfessel, Phys. Rev. Lett. **23**, 226 (1969)

[44]K. Y. Tsou and E. B. Hensley, J. Appl. Phys. **45**, 47 (1974).
[45]Ch. J. Raub, W. H. Zachariasen, T. H. Geballe, and B. T. Matthias, J. Phys. Chem. Solids **24**, 1093 (1963).
[46]Springer Materials, The Landolt-Börnstein Database [http://www.springermaterials.com].
[47]P. Diaz-Chao, I. J. Ferrer, J. R. Ares, and C. Sanchez, J. Phys. Chem. C **113**, 5329 (2009).
[48]H. Fischmeister, Acta Chem. Scand. **13**, 852 (1959).
[49]B. Radha and G. U. Kulkarni, Adv. Funct. Mater. **20**, 879 (2010).